This is a non-peer-reviewed preprint submitted to EarthArXiv.

The original version of this manuscript has been submitted for publication in Nature Geoscience on 22nd Mar 2024. The manuscript has now been formally accepted for publication. Subsequent versions of this manuscript may have slightly different content. When published, the final version of this manuscript will be available via the 'Peer-reviewed Publication DOI' link on the right-hand side of this webpage. Please feel free to contact any of the authors; we welcome feedback.

A fan-shaped subglacial basin province in East Antarctica formed by rotational extension

Egidio Armadillo[1]*, Daniele Rizzello[1]†, Pietro Balbi[1]‡, Alessandro Ghirotto[1]§, Davide Scafidi[2],
Guy J. G. Paxman[3], Andrea Zunino[4], Fausto Ferraccioli[5,6], Laura Crispini[2], Andreas Läufer[7],
Frank Lisker[8], Antonia Ruppel[7], Danilo Morelli[2] and Martin Siegert[9]

[1]Applied Geophysics Laboratory, DISTAV, University of Genoa, Genoa, Italy
[2]DISTAV, University of Genoa, Genoa, Italy
[3]Department of Geography, Durham University, Durham, United Kingdom
[4]Department of Earth and Planetary Sciences, ETH Zurich, Switzerland
[5]National Institute of Oceanography and Applied Geophysics (OGS), Trieste, Italy
[6]British Antarctic Survey (BAS), NERC, Cambridge, United Kingdom
[7]Federal Institute for Geosciences and Natural Resources (BGR), Hannover, Germany
[8]Department of Geosciences, University of Bremen, Bremen, Germany
[9] University of Exeter, Penryn, Cornwall, United Kingdom
*Corresponding author. Email: egidio.armadillo@unige.it
†Current address: Tellus-Explora S.a.s., Genoa, Italy
‡Current address: FS Engineering S.p.a., Genoa, Italy
§Current address: Department of Earth and Planetary Sciences, ETH Zurich, Switzerland

Abstract

Recent sub-ice topography investigations have imaged with greatly improved detail a set of low-elevation V- shaped basins hidden beneath a very large sector of the East Antarctic Ice Sheet. Here we jointly interpret sub-ice topography and geophysical data and show that these basins form a semi-continental sized fan shaped physiographic unit which radiates from a focal point near the South Pole. We name this the East Antarctic Fan-shaped Basin Province. We propose the fan-like landscape to be the product of distributed intraplate rotational extension prior to Gondwana breakup, with three continental-scale consequences. Laterally, to the west, it caused compression and the consequent uplift of the Gamburtsev Mountains. To the east, the northernmost Transantarctic Mountains segment was rotated clockwise of ~20° overriding the West Antarctic Rift System's hot lithosphere, causing segmentation of the mountain chain into three blocks and their differential uplift due to thermal buoyancy. To the North, the transcurrent edge of the fan formed the lithospheric weakness that controlled the break-up of Gondwana by driving the propagation of Antarctica/Australia separation and shaping the resulting semi-circular passive continental margins. These processes have influenced the present-day East Antarctica sub-ice landscape and the evolution of the overlying ice-sheet, including the development of glacial troughs and outlet glaciers.

MAIN TEXT

Antarctic bedrock is largely obscured by the Antarctic Ice Sheet, which covers more than 99% of the continent. Recently, international compilations of radio-echo sounding data[1,2,3] have resolved large-scale subglacial topographic features in increasing detail, revealing a wide and low-elevation sector of East Antarctica extending from Prydz Bay (70° E) to the Transantarctic Mountains (160° E) and from the coast inland to 85° S (Fig. 1). In this region, most of the large subglacial basins are V-shaped and aligned along the north-south direction. Moreover, the 2000 km long Antarctic coastline and continent-ocean boundary margin, delimiting the sector to the north, has a distinct semicircular arc geometry. At a semi-continental scale, the topography resembles a 'handheld fan', converging to a point located close to the South Pole (Fig. 1). We propose the whole region to be a single physiographic unit and name it the East Antarctic Fan-shaped Basin Province (EAFBP).

Here we document the geometry of the EAFBP, demonstrate its internal coherence, and propose that it formed through large-scale rotational extensional tectonics associated with Gondwana breakup. Because these basins underlie about half of the East Antarctic Ice Sheet, they are likely to influence heavily both ice-flow and landscape evolution[4,5], making them essential to Antarctic glacial and hydrological processes.

Sub-ice topographical observations

By detailed analysis of the subglacial morphological features (Methods) on the rebounded topography[3] (Extended Data Figure 1), we identified 30 basins comprising the EAFBP (Extended Data Table 1), all radially elongated along the north-south direction, with many exhibiting an approximately V-shape (Fig. 1). Together, the basins form a fan with an axis of symmetry passing through the Belgica Subglacial Highlands, aligned approximately along the meridian 130°E, here named the Belgica bisector. This bisector divides the EAFBP into the sinistral (SX) sector to the west and the dextral (DX) sector to the east.

To quantitatively define the geometry of the fan and estimate its pivot point location, we fitted the detected main longitudinal edges of the basins to great circles on the globe (Extended Data Figure 2 and Methods), represented in plan view by straight lines converging to the pivot point EP located at 86.4°S, 129.9°E (Fig. 1).

The EAFBP consists of two first-order symmetrically arranged V-shaped subglacial basins, the Wilkes and Aurora basins, which extend southward from the coastline for more than 1500 km. They appear to be dissected by a system of transverse east-west faults arranged along two circular belts, which we interpret as intraplate strike-slip shear belts[6], hereafter referred to as the southern and northern Transantarctic strike-slip Shear Circular Belts (Fig. 1). Along these belts, the Wilkes and Aurora basins show apparent dextral and sinistral offsets, respectively. These features may reflect genuine strike-slip motion, or alternatively, an apparent displacement of the extensional locus along pre-existing transverse structures. The two circular belts may be approximated on the Earth sphere by two small circles (Extended Data Figure 2 and Methods) whose pole locations (sEP: 84.2°S, 130.8°E; nEP: 83.1°S, 129.5°E) lie close to the fan pivot point EP, suggesting a common origin. The Wilkes and Aurora basin bed elevation also appears vertically offset across the two proposed strike-slip shear belts (Extended Data Figure 3), consistent with a vertical component of displacement.

The coastline marking the northern limit of the EAFBP forms an arc of a circle. On average, it may be interpolated from Cape Adare to Prydz Bay by a small circle (Extended Data Figure 2 and Methods) whose pole cEP is located at coordinates 81.7°S, 115.1°E, close to the previously estimated poles EP, sEP, nEP. Consequently, the two circular shear belts and the coastline divide the EAFBP into three annuli that we name as the southern, central and northern Transantarctic Annuli. Wilkes and Aurora basins cross all three annuli, while the other basins are confined within them.

The EAFBP is laterally delimited by two of the least understood mountain ranges on Earth (Fig. 1). To the west, the Gamburtsev Mountains are an intraplate subglacial range of uncertain origin[7,8] that exhibit unexpectedly youthful Alpine topography[7]. To the east, the Transantarctic Mountains are the largest non-compressional mountain belt in the world[9] separating East Antarctica from the West Antarctic Rift System[10] and dissected into multiple tectonic blocks[11,12,13].

The structural connection between the EAFBP and the Transantarctic Mountains is reflected in their topography. Approximately at the same latitude of the southernmost vertex of the Wilkes basin, between the Nimrod and Byrd glaciers, the Transantarctic Mountains exhibit a ~20° clockwise deflection relative to their southern linear trend. In addition, they appear segmented and right-laterally offset along both the Transantarctic strike-slip Shear Circular Belts forming three main distinct blocks (Fig. 1). Correspondingly, the West Antarctic Rift System grabens in the Ross Sea appear deflected clockwise[14] and right-laterally offset along the offshore continuation of the shear belts, even if there is no clear available evidence of dextral displacement along them.

The EAFBP onshore structure is also reflected in the facing oceanic structures along the Southern Ocean between East Antarctica and Australia (Fig. 2). Oceanic fracture zones are more closely spaced and prominent in correspondence with the main onshore structural lineaments in the EAFBP: the Transantarctic Mountains and the Wilkes basin to the east and the Lambert rift, SB1, Sabrina and Aurora basins to the west. Ridge offset variations (Fig. 2) identify five oceanic ridge segments: i) the Transantarctic Mountains – Wilkes basin segment, showing the strongest offsets in correspondence with the Balleny (continuation of the discontinuity between the Transantarctic Mountains and the West Antarctic Rift System), the George V (western Wilkes basin margin) and

Tasman (eastern Wilkes basin margin) fracture zones; ii) a central ‘quiet’ segment with very limited ridge offsets facing the Belgica bisector area; iii) the Sabrina-Aurora segment with a relevant but smoother distribution of the ridge offsets facing the two basins; iv) a second minor ‘quiet’ segment and v) the westernmost Lambert-SB1 segment with increased fracture zone spatial density and offsets.

Geophysical observations

The different rheological properties of distinct intracontinental blocks[12,15] may have controlled rotational extension within the EAFBP. The Lake Vostok trough is formed by a major geological boundary that is partially coincident with the proposed Mawson continent western flank[12] (Western Mawson Suture) and appears to delimit the Aurora basin to the west. The western flank of the Wilkes basin features a sharp magnetic[16,17] and gravimetric[18] break that defines the boundary (Eastern Mawson Suture) between the thick and highly magnetic Mawson continent of the East Antarctic Cratonic Assemblage[19] and the thinner and weakly magnetic Ross Orogen Belt[12,16] (Fig. 2).

The fan-shaped structure is also recorded in the lithosphere. A crustal depth model[20], based on integrated seismic and gravimetric data, indicates thinned crust corresponding to the major basins in the EAFBP (Extended Data Figure 4). At the same time, previously unrecognized, low-velocity anomalies under the Wilkes and Aurora Subglacial Basins have recently been imaged[21], suggesting a radial pattern of thinner than expected lithosphere, thermally perturbed upper mantle and anomalous geothermal heat flux.

The kinematic model

Candidate processes that may have operated in the study area and generated the EAFBP semi-continental scale fan-like structural pattern include glacial erosion and extensional tectonic deformation (e.g., rotational extension[22-24], rift propagation[25] and structural control by inherited structures[26]). We discount glacial erosion as the primary mechanism shaping the observed topography because contemporary ice surface velocities[27] across the study area (Extended Data Figure 5) are generally low (<10 m/yr) and geomorphological evidence suggests that glacial erosion by earlier ice sheets in the East Antarctic interior was selectively focused through existing valleys on a smaller scale than the features comprising the EAFBP[28]. We also consider rift propagation mechanisms unlikely here because they typically affect spreading centers at mid-ocean ridges and back-arc basins[25]. Finally, although inherited structures may have influenced fault localization, the coherent continent-scale radial pattern argues against structural inheritance alone and instead requires a broader genetic mechanism. This interpretation is supported by the spatial coincidence between the inferred radial focal point and the pole of the small circle approximation of the present-day continent-ocean boundary (Fig. 1), and by the link between inland lineaments and major oceanic fracture zones (Fig. 2).

We therefore developed a conceptual kinematic model that interprets the observations presented (summarized in Extended Data Table 2) in terms of rotational extension, a mechanism widely invoked to explain similar large-scale radial structural patterns elsewhere in the world[22-24]. In plan view, the process is analogous to the opening of a folding fan and thus requires a pivot point and a fixed central arm, from which the two sides of the fan move away (Extended Data Figure 6). The resultant kinematic model is simplified into two phases sketched in Fig. 3 (additional details are given in Supplementary Information paragraphs 1 and 2).

At the initial stage (Fig. 3A), counter-clockwise fan-shaped extension around the pivot point EP formed the Aurora basin, while simultaneous clockwise extension formed the Wilkes basin, forming a large sphenochasm within the continental crust.

The fanning out propagated from the Belgica bisector, while the basins master faults' locations were controlled by the existing lithospheric discontinuities made by the Eastern and Western Mawson sutures. In our model, northward deepening of the Wilkes and Aurora basins (Extended Data Figure 6) was accommodated by two major east-west normal faults, possibly reactivated from Neoproterozoic lithospheric discontinuities[13]. The western side of the Wilkes basin coincided partially with the Eastern Mawson Suture and remained unaffected by the subsequent dextral offset, whereas the eastern side of the Aurora basin partly matched the Western Mawson Suture and was likely affected by the subsequent sinistral offset. As result, the Mawson continent evolved into its present-day wedge-shaped geometry. Within the rotational extension framework, the ~20° deflection observed in the Transantarctic Mountains is interpreted as a rotation consistent with the position of the fan pivot point (EP). The deflection point, between the Nimrod and Byrd glaciers, likely coincide with inherited main fault structures that accommodated the rotational extension by both vertical and strike-slip movements. This area corresponds to a previously observed but unexplained lithospheric discontinuity[14] in the Transantarctic Mountains and Ross Sea.

At a later stage (Fig. 3B), as fan extension increased, progressive northward basement lowering was partly relieved by the opening of secondary basins/trenches within the central and northern annuli, between the two strike-slip shear belts localized along the original east-west lithospheric breaks in the Wilkes and Aurora basins. In our model, these lithospheric breaks initially controlled basin subsidence, but later evolved into zones of transverse strike-slip motion (Supplementary Information paragraph 3) as rotational extension intensified, thereby partitioning the northward increase in extensional strain, as observed in similar settings[29]. Alternatively, the transverse offsets could represent transfer faults that shift the focus of extension without true strike-slip motion, although we consider this explanation less probable.

In our interpretation, the increasing extensional strain towards the North accommodated along the shear belts, likely caused the segmentation of the Transantarctic Mountains into the three observed blocks (Fig. 1) and the corresponding segmentation of the extensional features in the West Antarctic Rift System. The three Transantarctic Mountains blocks overrode the hot lithosphere of the West Antarctic Rift System, and underwent additional differential uplift in time and space due to differential thermal buoyancy[9] (Extended Data Figure 7).

To the west, our model suggests that rotational extension has only weakly affected the area beyond the Western Mawson Suture likely because of the originally thicker crust and lithosphere[20,21] (Extended data Figure 4). In this area extension was focused along deep and narrow trenches such as Lake Vostok and the East Antarctic Rift System. However, the fanning out likely reactivated the Lambert Rift and, in the later stage, offset the East Antarctic Rift System. We propose that the rotational extension in the EAFBP was, at least partially, accommodated by compression in the Gamburtsev Mountains region causing additional uplift and contributing to their youthful Alpine topography[7].

To the north, observations are consistent with a scenario in which the EAFBP fanning out generated the semi-circular lithospheric weakness line that controlled Antarctica-Australia separation. In our model, the inferred EAFBP transcurrent releasing fault system representing the northern fan limit evolved from a semi-circular diffuse principal displacement zone into a set of *en-échelon* strike-slip faults (Fig. 4). The most prominent of these faults originated from bending of existing major lithospheric discontinuities, such as the Eastern and Western Mawson sutures and the Transantarctic Mountains - West Antarctic Rift System discontinuity and/or of the major longitudinal coastal basins' master faults.

At a later stage of the proposed scenario, approximately east-west pull-apart basins developed along the northern EAFBP edge between consecutive overlapping strike-slip faults and may have evolved into short seafloor spreading segments with large offset between them. During the subsequent Antarctica/Australia rifting, these pull-apart basins may have driven west to east ridge propagation producing the transfer faults responsible for the present-day fracture zone distribution and partitioning of the Southeast Indian Ridge into five segments (Fig. 2). The final effect was the semi-circular geometry of the conjugated Antarctic/Australian margins. The deviation towards north-west of the Eastern Mawson Suture at the coastline together with inferred strike-slip faults marked by canyons and scarps in the continental slope and platform facing the main fracture zones in the oceanic crust (Fig. 2), may preserve evidence of the proposed process. We have compiled a comprehensive list of supporting evidence for the proposed mechanism in the Supplementary Information paragraph 4.

Timing of the rotational extension

The extensive ice-sheet cover preventing direct observations in the inner continent, together with uncertainties about the age and evolution of the Transantarctic Mountains and the West Antarctic Rift System[10,12,13], make it difficult to estimate when and for how long the EAFBP was active. Rotational extension might have occurred during known tectonic plate re-arrangements or major extension episodes: (i) in the Late Paleozoic–Triassic, when a major denudation event occurred[30], (ii) during Gondwana breakup in the Jurassic–Cretaceous and early Cenozoic[31], and/or (iii) in the Eocene with possible transcurrent sinistral offsets along the eastern rift margin[32]. The fanning out may have also been superimposed on the intra-Gondwana Mesozoic Victoria Basin[33] and may have been multiphase. Independent thermochronological evidence from the continental interior of subglacial East Antarctica indicates cooling and exhumation during the Cretaceous[34] (ca. 90–100 Ma). In addition, Cenozoic reactivation of Antarctic rift zones has been linked to localized upper-mantle thermal anomalies beneath Antarctica[35], suggesting that both lithospheric architecture and mantle-driven processes may have contributed to the development and reactivation of the inferred fan-shaped extensional system.

Tectonic and glacial legacy in East Antarctica

According to the proposed model, the "handheld fan" shaped feature in the East Antarctic landscape originated through a single continental scale process driven by rotational extension. This process profoundly reworked pre-existing structures and influenced the development of later continental scale features. It may have triggered additional uplift of the Gamburtsev and Transantarctic mountains, segmented the Transantarctic Mountains and the West Antarctic Rift System and formation of the semicircular conjugated margins between Antarctica and Australia. It may therefore have played a key role as precursor of Gondwana breakup, with implications for tectonic reconstructions and geodynamic models linking onshore structures to offshore fracture zones.

Furthermore, the approximate coincidence between the fan's pivot pole and the Euler poles proposed for East/West Antarctica extension[36] after ~34 Ma (Extended Data Figure 2), when uncertainties in pole location are taken into account, raises questions about the long-term stability of deformation poles and their potential role in linking continental rifting processes to subsequent plate motions. Since no evidence of EAFBP continuation is found in Australia, the fan-like rotational extension must have been confined to the Antarctic lithosphere. Recognition of this intra-plate deformation can therefore inform new plate reconstructions of the Australia-Antarctica fit, potentially accounting for the anomalously large crustal overlaps reported in some models[37,38] and for mismatches in the correlation of basement terranes and major faults across the two conjugate margins[31,39].

The proposed tectonic scenario may also have influenced the onset and evolution of the East Antarctic Ice Sheet (additional details in Supplementary Information paragraph 5), which nucleated at about 34 Ma. Over the EAFBP region, the volume of ice has a sea level equivalent of 28 m. Sedimentary basins interact with the overlying ice sheet through dynamic feedbacks known to affect ice-sheet retreat dynamics[4]. Following extension, cooling, and subsidence, the resulting topographic surface may locally lie below modern mean sea level, potentially enhancing the long-term sensitivity and vulnerability of the ice sheet. The segmentation of the Transantarctic

Mountains along the east-west circular shear belts was likely subsequently exploited by major outlet glaciers such as Byrd, Beardmore, Nimrod, David, Priestley and Tucker, incising deep glacial troughs that in turn caused further isostatic uplift of the mountain peaks. Similarly, the major north-south fan shaped structural boundaries of the basins within the EAFBP appear to control the locations of major outlet glaciers around the East Antarctic margin, including Totten, Vanderford, Denman, Frost and Amery. This association implies direct tectonic control on ice sheet behavior and highlights the importance of geological processes initiated ~ 150 million years ago in modulating ice sheet dynamics today and in the future.

Acknowledgments

This research was conceived at the Applied Geophysics Laboratory of the University of Genoa, then led by Emanuele Bozzo and including Giorgio Caneva.

Funding and support were provided by the Italian National Research Program in Antarctica (PNRA grants 2009/A2.03-BABOC, 2010/A2.01-ISEE, PNRA19_00051-A1-BOOST: EA, LC, AG, PB, DR, DM) and by the University of Genoa (grants Fondi Ricerca Ateneo FRA 2022 and 2023: EA). Additional support came from the German Research Foundation and the Special Priority Programme "Antarctic Research with Comparative Investigations in Arctic Ice Areas" (grants LI 745/8, LI 745/12, LI 745/26, LA 1080/7 and LA 1080/19: AL, AR).

The maps presented in this paper were generated using Seequent Oasis montaj, and the figures were prepared and refined using CorelDRAW.

Author contributions:

Conceptualization: EA

Methodology: EA, DR, PB, AG, DS, GP, AZ

Investigation: EA, DR, PB, AG, DS, AZ

Visualization: EA, DR, PB, AG, DS, AZ

Funding acquisition: EA, LC, AL

Supervision: MS, EA, AZ, GP, FF, LC, AL, FL, AR, DM

Writing – original draft: EA

Writing – review & editing: all

Competing interests

Authors declare that they have no competing interests.

Figure Legends/Captions (for main text figures)

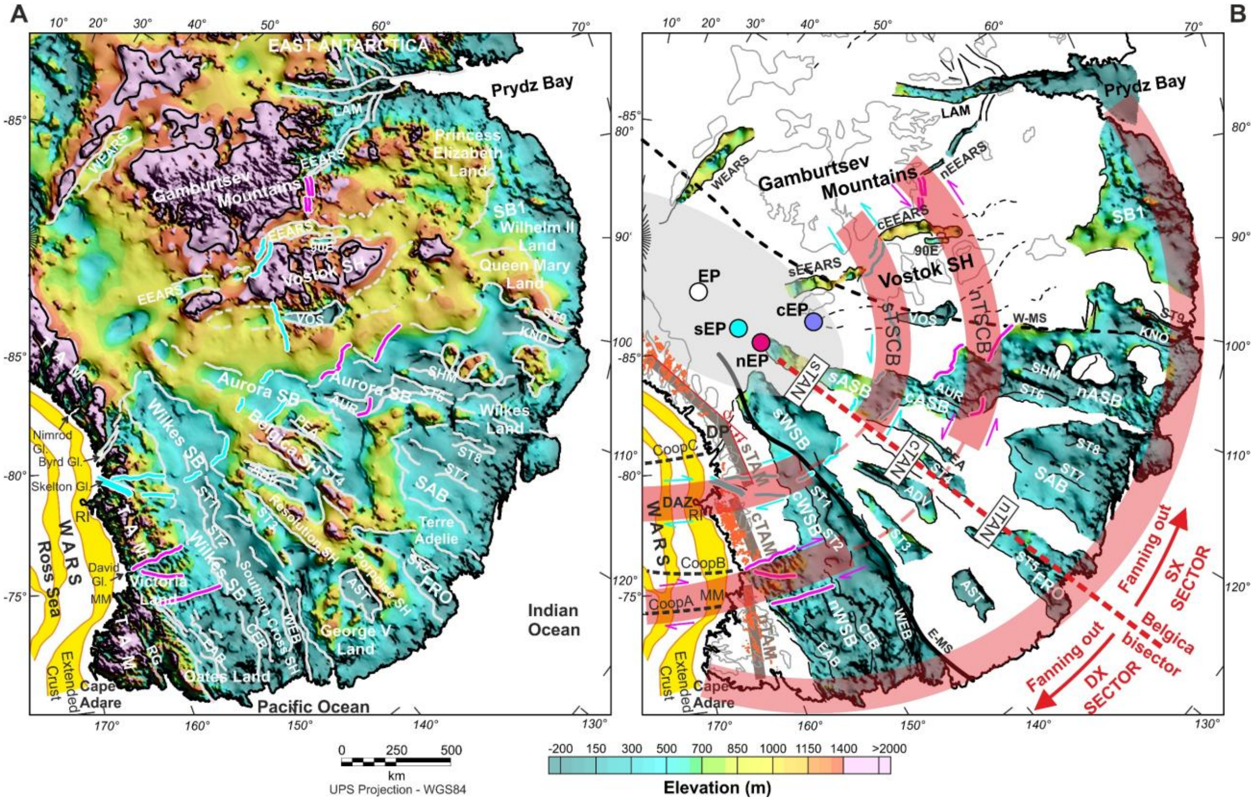

Figure 1

Fault-controlled basins and interpreted structural frame in the newly identified East Antarctic Fan Basin Province.

(A) Sub-ice topography corrected for isostatic rebound due to ice removal[3] with sharp topographic features enhanced by non-linear filtering (Methods). Light gray lines are detected topographic lineaments interpreted as longitudinal normal faults forming the structural edges of the basins. Magenta and cyan lines are detected topographic lineaments interpreted as either transverse strike-slip faults or associated normal faults that characterize the two circular shear belts sTSCB and nTSCB shown in (B). The acronyms of the basins are listed in Extended Data Table 1. The yellow bands in the Ross Sea outline highly-extended crust mapped from depth to basement and gravity anomalies[40]. Black contour line represents 1500 m elevation. MM: Mount Melbourne. RI: Ross Island. RG: Rennick Graben. WARS: West Antarctic Rift System.

(B) Main structural features of the East Antarctic Fan Basin Province. sTSCB, nTSCB: principal displacement zone of the southern and northern Transantarctic strike-slip Shear Circular Belts. sTAN, cTAN, nTAN: southern, central and northern Transantarctic Annuli. EP, sEP, nEP, cEP: estimated Euler pole from the edges of the basins (EP, error ellipse in light gray), from the structures associated to the sTSCB (sEP) and nTSCB (nEP) and from the coastline (cEP) between Cape Adare and Prydz Bay (Methods). CoopA, CoopB, CoopC: mapped major lithospheric discontinuities in the Ross Sea[14]. DP: deflecting point of the Transantarctic Mountains (TAM) indicating rotation with respect to their southern original trend. α: clockwise TAM rotation angle of about 20°. sTAM, cTAM, nTAM: TAM blocks formed by the offset along the sTSCB and nTSCB. E-MS: magnetic and gravimetric signature of the Eastern Mawson Suture[16,17]. W-MS: inferred Western Mawson Suture[12]. DAZ: Discovery accommodation zone[41]. Orange dots indicate outcrops of the Jurassic Ferrar Supergroup[42]that appear offset in three blocks as the TAM. Grey contour line represents 1500 m topographic elevation.

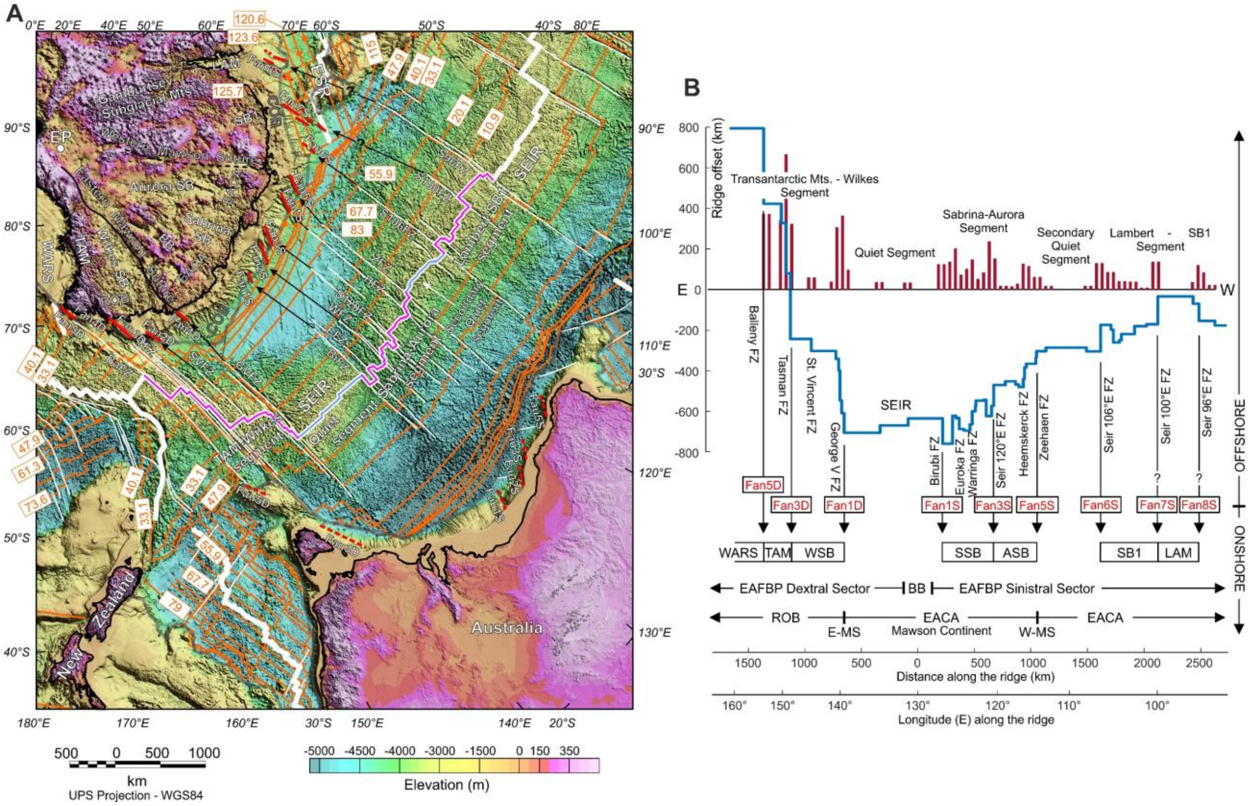

Figure 2

Offshore fracture zone distribution relative to the onshore location of the basins in the EAFBP.

(A) Present day configuration of the Antarctica-Australia rifted margin and main fracture zones[43,44] superimposed on the ETOPO Global Relief Model[45]. The correspondence of the offshore fracture zones (FZ) with the onshore coastal EAFBP basins' margins is obtained prolonging the FZ towards the Antarctic passive continental margin. Fan1D-Fan5D, Fan1S-Fan8S: canyons and scarps in the East Antarctica continental slope with a different trend than the maximum slope direction. Fau1D-Fau5D, Fau1S-Fau8S: tentatively inferred continuations on the Australian margin of the Antarctic strike-slip Fan fault system. SEIR: Southeast Indian Ridge. ESR: extinct spreading ridge[46]. BaFZ: Balleny FZ; TFZ: Tasman FZ; SVFZ: St Vincent FZ; GVFZ: George V FZ; BiFZ: Birubi FZ; EFZ: Euroka FZ; WFZ: Warringa FZ; S120FZ: Seir120E FZ; HFZ: Heemskerck FZ; ZFZ: Zeehaen FZ; S106 FZ: Seir106E FZ; S100FZ: Seir100E FZ; S96FZ: Seir96E FZ. White thick lines: oceanic ridges[47]; white thin lines: main fracture zones[43]; orange lines: isochrons[48], years reported in Ma; thick gray lines: continental ocean boundaries[49]. COB: continent-ocean boundary. TAM: Transantarctic Mountains. WARS: West Antarctic Rift System. EACA: East Antarctic Cratonic Assemblage; ROB: Ross Orogen belt. Note that the relationship between the faults Fan7S and Fan8S with Seir100E and Seir96E FZs is more uncertain due to the greater distance between them.

(B) Blue line: SEIR offsets[47] along the fracture zones vs. the distance along the ridge; the zero of the offset scale is arbitrary, the zero of the distance along the ridge is the Belgica bisector (BB). Dark red lines: histogram representing the sum of the absolute values of the ridge offsets computed over a running window 100 km long with 50% of overlap between consecutive windows; bars are therefore proportional to the SEIR offset for unit distance. W-MS, E-MS: Western and Eastern Mawson sutures. Note the larger offsets of the SEIR in correspondence with the onshore EAFBP basins' limit in the continental crust. Also note the large difference in the offsets' trend for the FZs facing the onshore EACA and ROB domains and the consequent difference in the curvature of the coastline and COB.

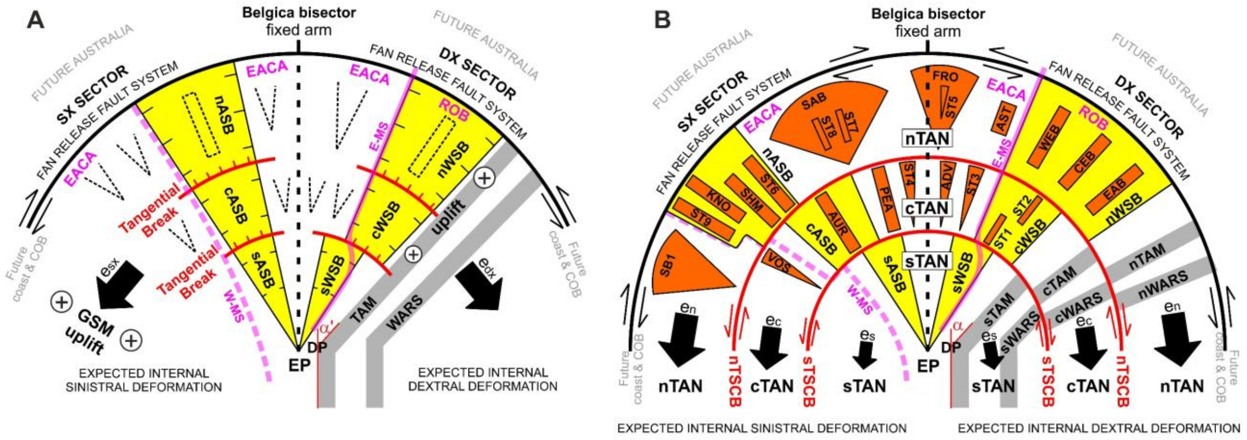

Figure 3

Proposed two-phase kinematic conceptual model of formation of the EAFBP (not to scale).

(A) Initial phase with the formation of the major 'twin' Aurora and Wilkes basins caused by rotational movements around the Euler pole EP, symmetrical with respect to the Belgica bisector. Tangential normal faults (thick red lines) are formed in the two basins to accommodate the northward increasing depth. The Transantarctic Mountains (TAM) and the West Antarctic Rift System (WARS) are rotated clockwise by an angle α'. Secondary basins (V-shaped and rectangular basins, dashed lines) open in the external annuli of the fan, to maintain the basin distribution for unit area approximately constant. To the west, the extension is accommodated by compressional reactivation of the Gamburtsev Mountains (GSM) uplift, which also occurs in the later phase. To the east, the TAM are pushed over the hot WARS lithosphere and undergo differential uplift (Extended Data Figure 7). In this phase the Western Mawson Suture (W-MS) is bended anticlockwise; the Eastern Mawson Suture (E-MS) preserves its original orientation owing to its closeness to the Belgica fixed arm. EACA: East Antarctic Cratonic Assemblage; ROB: Ross Orogen belt; E-MS: Eastern Mawson Suture; W-MS: Western Mawson Suture; DP: TAM deflection point.

(B) Later phase with increasing opening of additional secondary basins and start-up of the lateral offsets along the southern and northern Transantarctic strike-slip Shear Circular Belts (sTSCB and nTSCP). The fan is divided into two sectors with dextral (DX) or sinistral (SX) shear and three annuli (the southern, sTAN, central, cTAN, and northern, nTAN, Transantarctic Annuli). The additional extensional strain increases in the three annuli from south to north ($e_s < e_c < e_n$). The shear along the three annuli segments the WSB and ASB in three parts (sWSB, cWSB, nWSB, sASB, cASB, nASB). Also, the TAM are segmented in three blocks (sTAM, cTAM, nTAM) and the same applies to the WARS (sWARS, cWARS, nWARS). To the north, the EAFBP is terminated by a dextral (in the SX sector) or sinistral (in the DX sector) transcurrent release fault system made up of *en-échelon* strike-slip faults shown in Fig. 4. The final rotation angle of the TAM around point DP is α ≅ 20°.

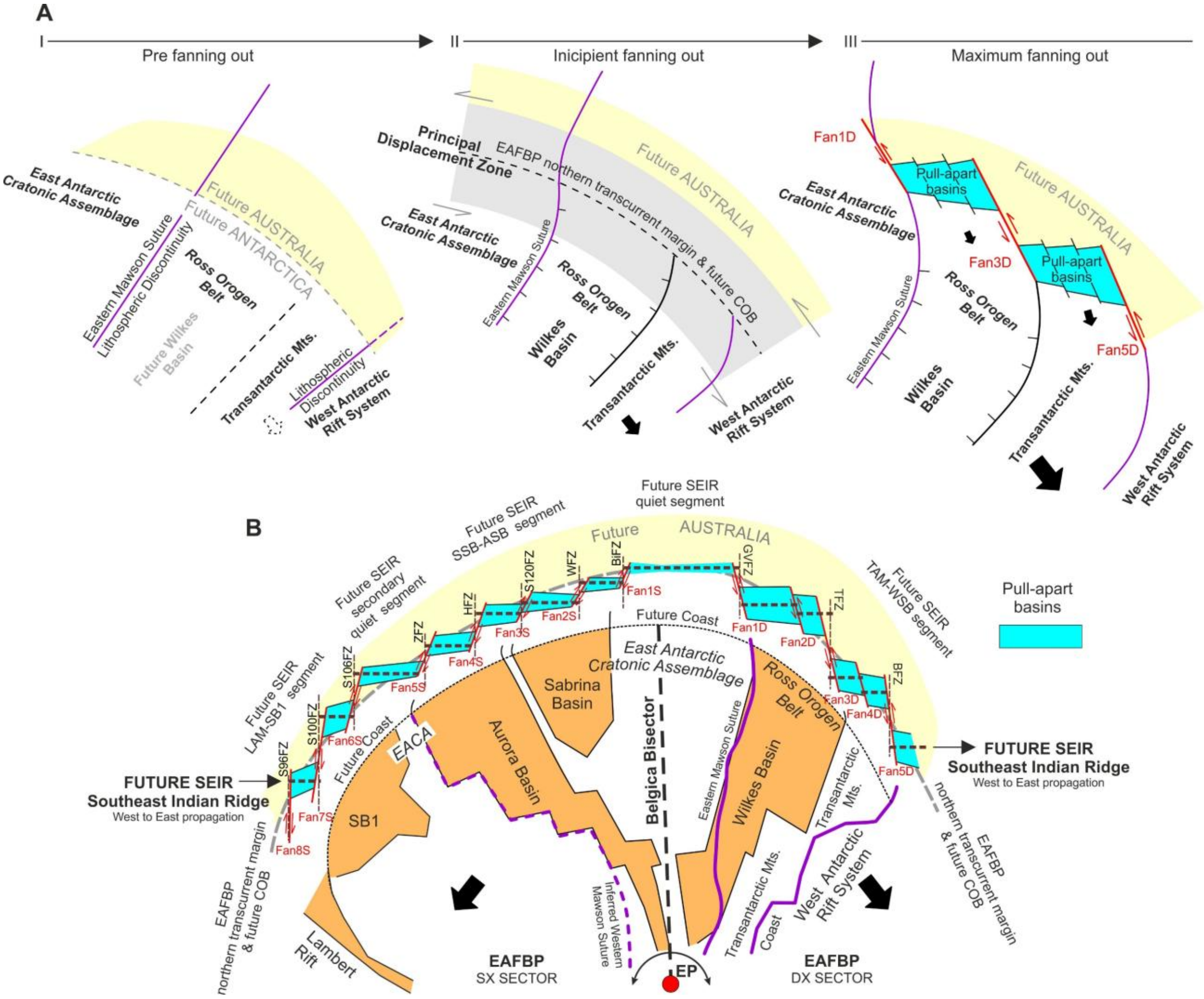

Figure 4.

Evolution of the northern EAFBP release-fault system and its control on margin curvature and fracture zones.

(A) Proposed evolution of the northern EAFBP transcurrent fault-release system along the dextral sector; a specular evolution is expected in the sinistral sector. (I) Pre-existing lithospheric discontinuities are assumed. (II) During incipient fanning out, these discontinuities and/or newly formed longitudinal normal faults are laterally deformed along the sinistral principal displacement zone accommodating rotational extension against fixed future continental Australia. (III) With increasing extension, overlapping *en-échelon* left-lateral strike-slip faults (Fan1D, Fan3D, Fan5D) develop, generating asymmetric pull-apart basins that may evolve into short seafloor-spreading segments.

(B) Final configuration of the northern EAFBP transcurrent fault-release system. Increasing lateral offset away from the Belgica bisector generates east-west pull-apart basins, guiding future rift propagation, orthogonal fracture zones, and the geometry of the future Continent Ocean Boundary

(COB) and coastlines at the conjugated Antarctic-Australian margins. In the dextral sector, deformation is localized by lithospheric discontinuities at the East Antarctic Cratonic Assemblage, Wilkes Subglacial Basin, Transantarctic Mountains and West Antarctic Rift System boundaries. Combined with thinner Ross Orogen Belt lithosphere, this produces greater offsets, higher extensional strain, and stronger COB curvature than in the sinistral sector.

EXTENDED DATA FIGURES AND TABLES

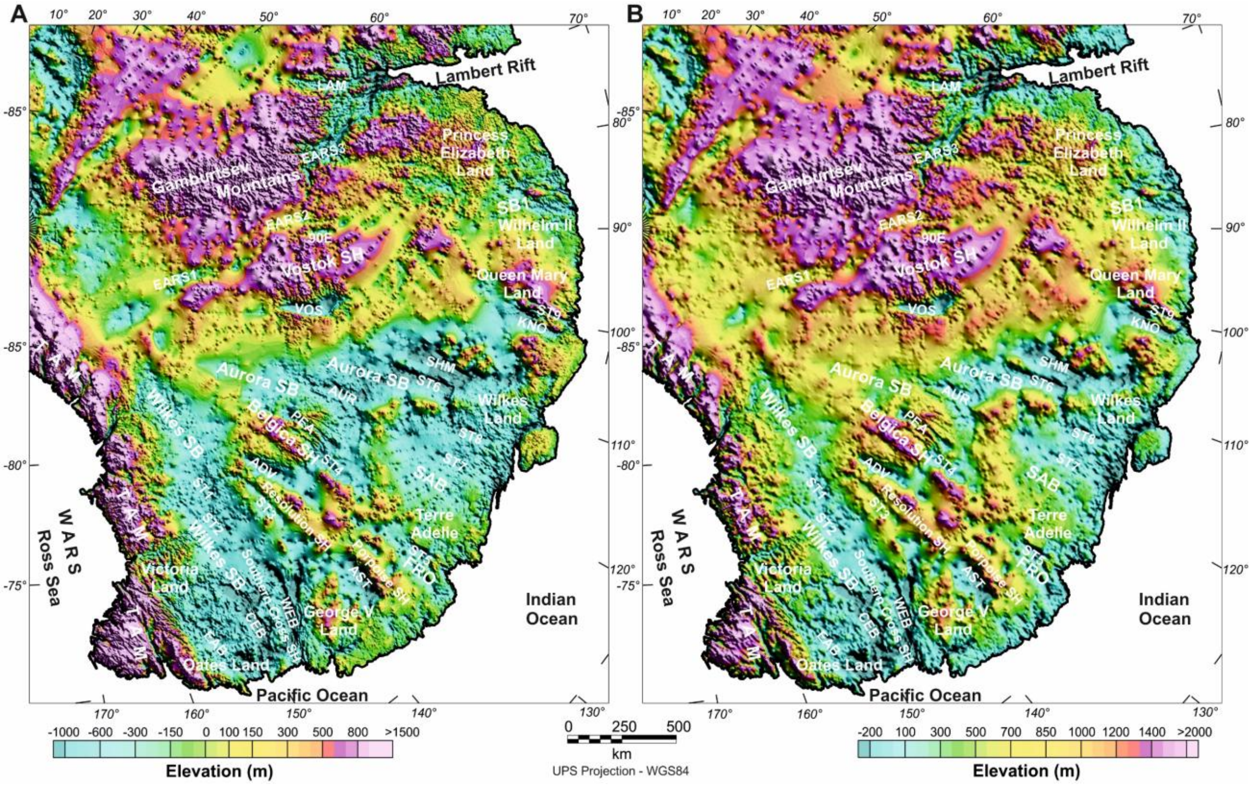

Extended Data Fig. 1

(A) BedMachine[2] sub-ice topography.

(B) Adjusted topography for the isostatic effect of ice sheet removal[3], obtained computing the flexural response to the complete removal of the modern grounded ice load using an elastic plate model with a laterally variability flexural rigidity and accounting for the disequilibrium associated with the ongoing response to ice mass changes since the Last Glacial Maximum. The original grid has been down-sampled to 5000 m. Note the different color scales in the two maps.

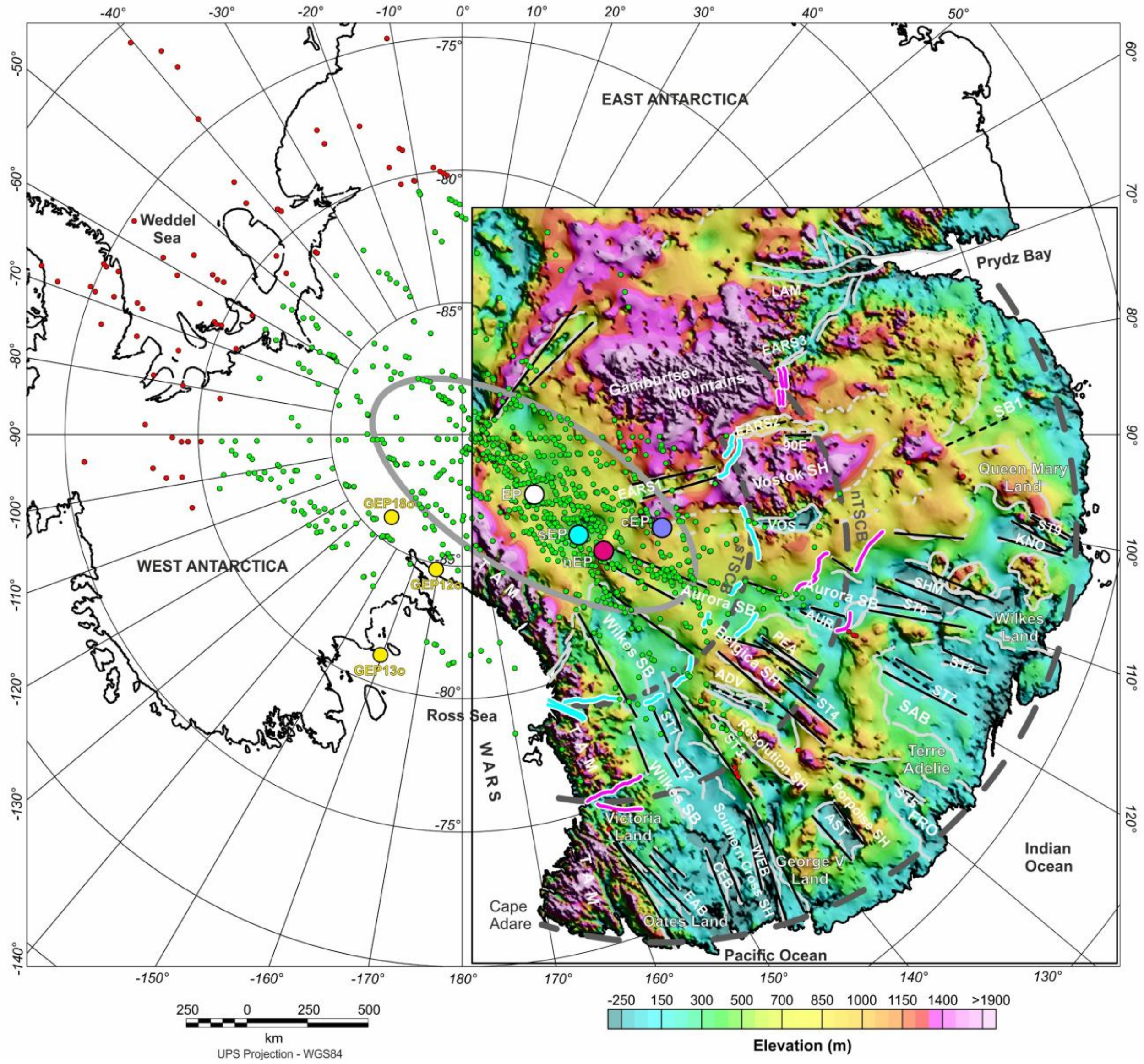

Extended Data Fig. 2

Topographic lineaments identified by the semiautomatic analysis of the filtered rebounded topography[3] (color map; see Methods) are interpreted as approximately north-south normal faults (light gray lines) and approximately east-west strike-slip faults with associated transtensional conjugate faults (cyan and magenta lines). The longitudinal normal faults (light gray lines) were fitted with great-circle segments (black straight lines), and their intersections were calculated (small red and green circles). The pivot point EP (large white circle) was estimated as the mean location of the green intersection points, whereas the red intersection points were discarded. The error ellipse (light gray line) is the minimum-area ellipse containing 68% of the green intersection points. The east-west transverse strike-slip faults, or dominant east-west normal faults related to transtension, defining the nTAN shear belt (magenta lines), were fitted by a small circle (dashed dark gray line), whose Euler Pole (nEP) is shown by a large magenta circle. The corresponding faults defining the sTAN shear belt (cyan lines) were also fitted by a small circle (dashed dark gray line), whose Euler Pole (sEP) is shown by a large cyan circle. The coastline was fitted by a small circle (dashed dark gray line), whose Euler Pole (cEP) is marked by a large violet circle. The three additional Euler poles (sEP, nEP, and cEP) fall within the EP error ellipse. GEP12o, GEP13o, and GEP18o denote the best-fit rotation poles^36 for relative motion between East Antarctica (fixed) and West Antarctica at magnetic subchrons 12o (30.9 Ma), 13o (33.5 Ma), and 18o (40.1 Ma), respectively.

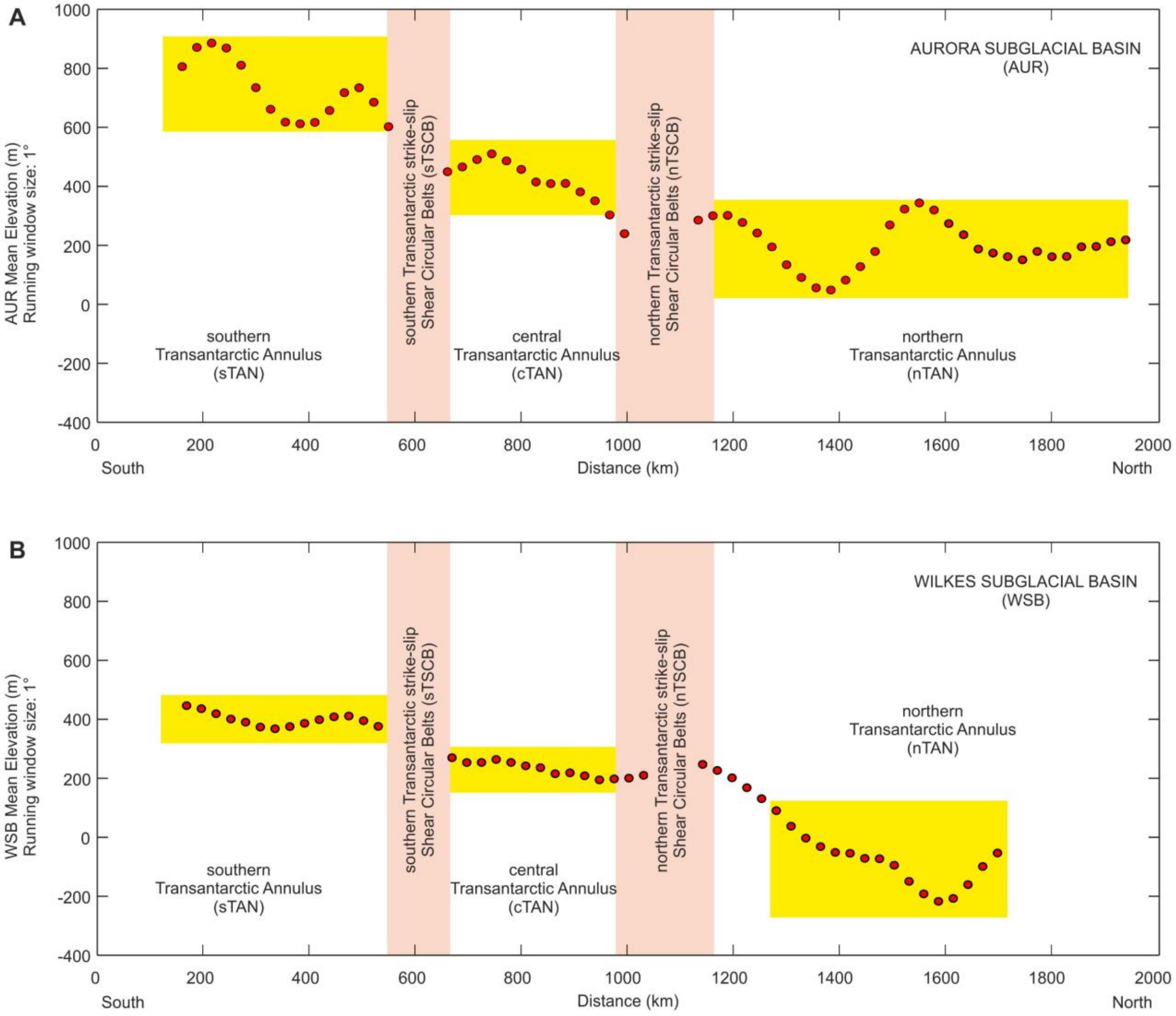

Extended Data Fig. 3

Mean bed elevation (red dots; rebounded topography) was calculated in circular running windows defined by 1° annuli centered on the mean positions of the sEP and nEP poles. The horizontal axis reports the distance (km) of each window from the corresponding mean pole. The southern and northern Transantarctic strike-slip Shear Circular Belts (sTSCB and nTSCB; pink areas) subdivide the Wilkes and Aurora basins into three main sectors, corresponding to the southern, central, and northern Transantarctic Annuli (sTAN, cTAN, and nTAN). Mean bed elevation across these annuli defines three distinct levels (yellow bands), rather than a linear trend. In the Wilkes Basin, a third topographic step may occur at ~1500 km, possibly marking the northern limit of the EAFP transform fault, although this interpretation may be affected by strong glacial erosion near the coastline.

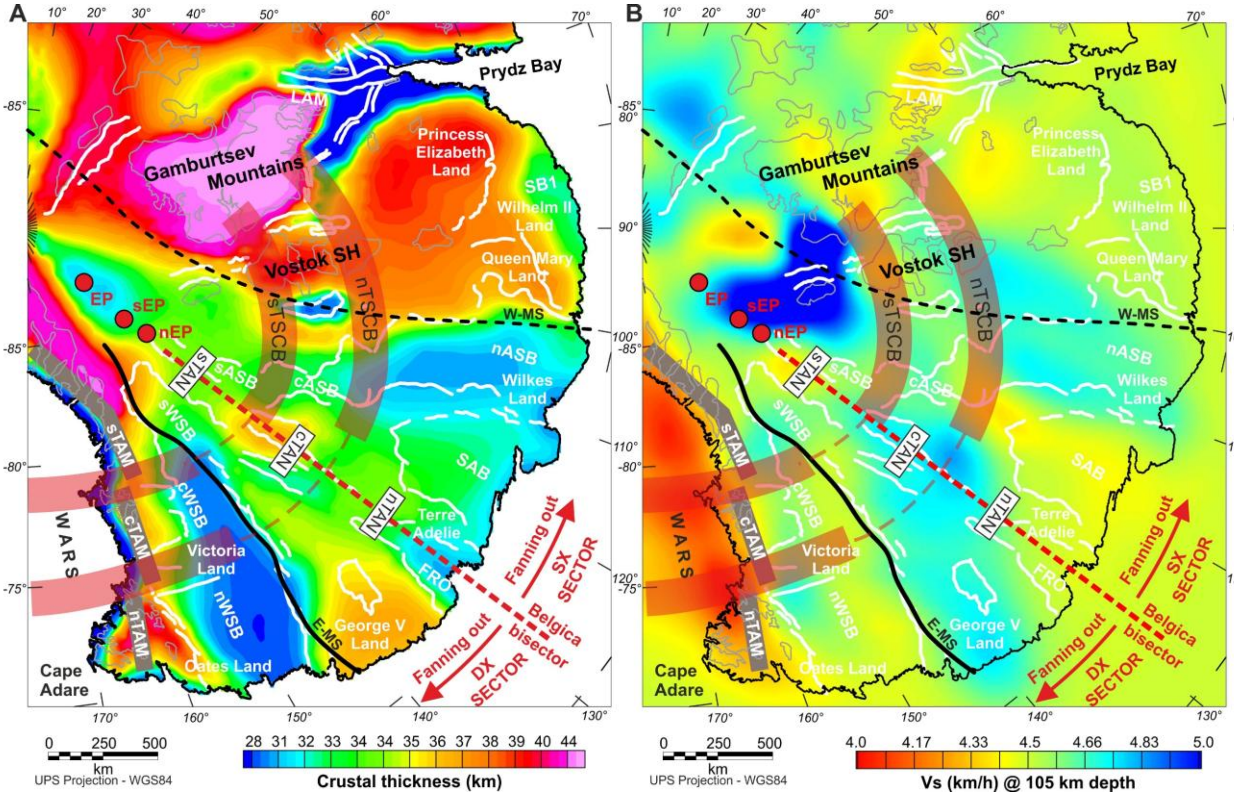

Extended Data Fig. 4

(A) Main structural features of the EAFBP superimposed on the crustal thickness map derived from joint analysis of gravity and seismic data[20]. Reduced crustal thickness beneath the main EAFBP basins is consistent with rotational extension. The segmentation and offset of the TAM into three blocks (sTAM, cTAM, nTAM) inferred from topographical and geological evidence is also expressed in the crustal thickness pattern. E-MS: Eastern Mawson Suture. W-MS: Western Mawson Suture. EP: EAFBP pole. sEP, nEP: poles of the southern and northern Transantarctic strike-slip Shear Circular Belts. White heavy lines: main basins in the EAFBP.

(B) Main structural features of the EAFBP superimposed on the shear-wave velocity anomalies at 105 km depth derived from full-waveform ambient-noise tomography[**Error! Reference source not found.**].

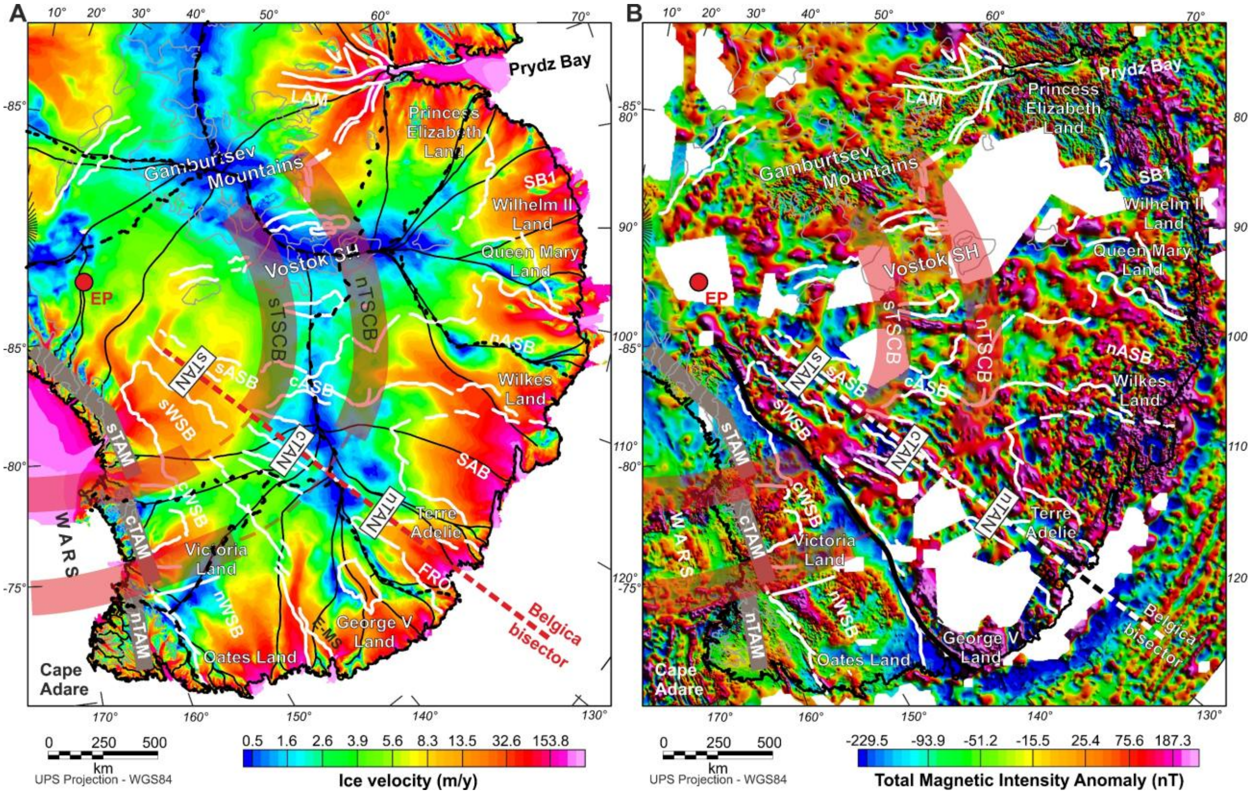

Extended Data Fig. 5

(A) Ice velocity map and and ice basins' divides[27].

(B) Total Magnetic Intensity map[17]

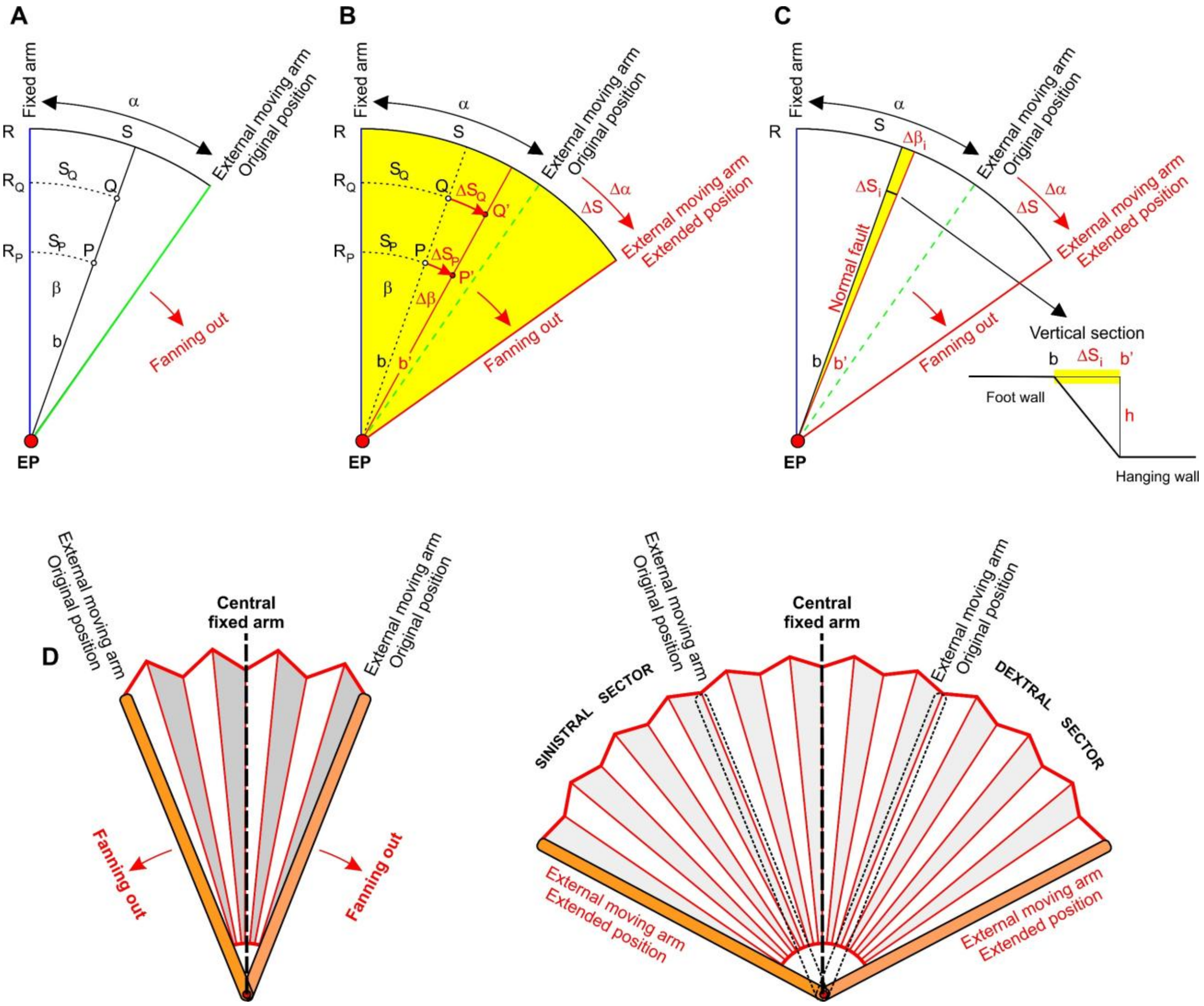

Extended Data Fig. 6

(A) Folded fan before extension; only the right sector is shown for simplicity. The angle between the fixed arm and the outer arm is α, and the length along the external arc is S. P and Q are points along the same stick b of the fan at a distance (along the arc) SQ and SP and angular distance β from the fixed arm. RP and RQ are the distance from the pivot point EP.

(B) Folding out of the fan to the right, in the case of continuous deformation. The external moving arm is rotated clockwise by an angle $\Delta\alpha$ that corresponds to the length Δs along the arc. The ratio $e=\Delta\alpha/\alpha=R\Delta\alpha/R\alpha=\Delta S/S$ defines the extensional strain of the fan. The internal stick b is rotated in b' by an angle $\Delta\beta$ such that $e=\Delta\beta/\beta$. The two points P and Q are displaced in P' and Q', following a trajectory along the arcs of radii RP and RQ. The displacements ΔS_P and ΔS_Q are such that $e=\Delta S_P/S_P=\Delta S_Q/S_Q$. Note that, along the same stick, the displacement increases moving away from EP: $\Delta S_Q>\Delta S_P$ when $R_Q> R_P$.

(C) Folding out of the fan to the right, in the case of brittle deformation accommodated by a set of radial normal faults (only one is drawn) forming the longitudinal edges of the main basins. Each normal fault contributes to accommodate the total extension $\Delta\alpha$ by a small angle $\Delta\beta_i$. The increasing linear displacement ΔS_i moving away from EP implies an increasing vertical displacement h along the fault and a consequent increasing sinking of the hanging wall.

(D) Analogy between the rotational extension model and opening of a handheld fan

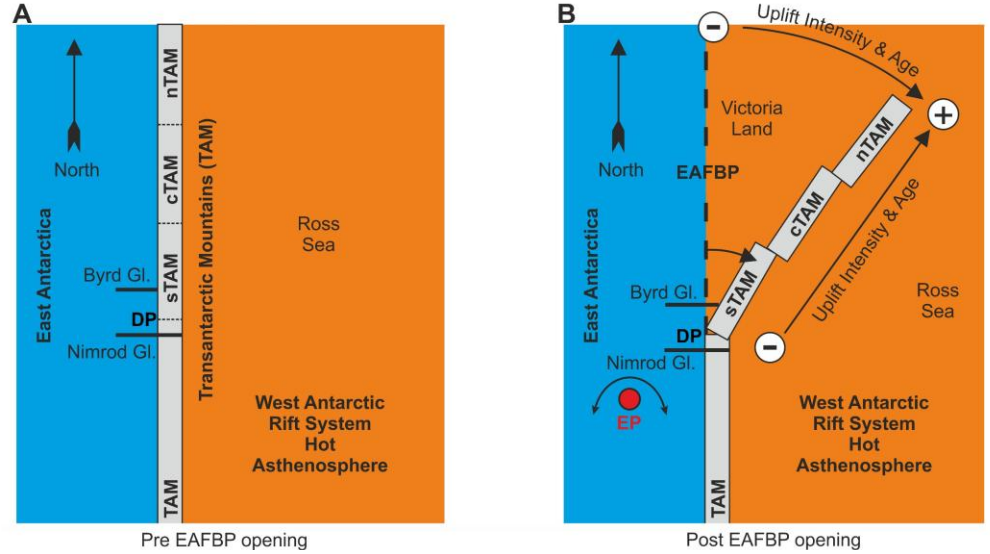

Extended Data Fig. 7

(A) Pre EAFBP configuration. NG: Nimrod Gl.; BG: Byrd Gl.

(B) Post EAFBP fan opening. The fanning out of the EAFBP displaced the sTAM, cTAM and nTAM blocks eastward, overriding the hot West Antarctic Rift System lithosphere. Due to the rotational extension, the northernmost nTAM sector was the first to override the WARS lithosphere and reached the easternmost position, resulting in greater thermal buoyancy. Accordingly, the additional uplift is expected to be older and more intense toward the coastal sector of the nTAM, and to decrease inland, consistent with some interpretations of apatite fission-track thermochronology**Error! Reference source not found.Error! Reference source not found.**. Southward along the coast, across the cTAM and sTAM blocks, the additional uplift is instead expected to become progressively weaker and younger.

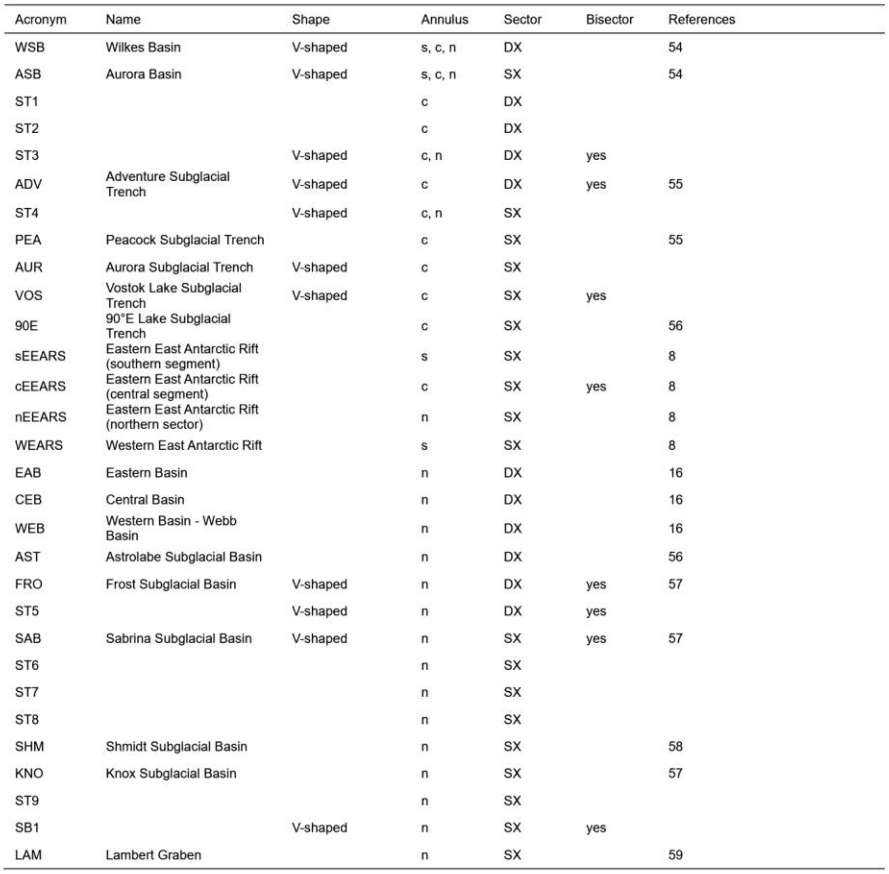

Acronym	Name	Shape	Annulus	Sector	Bisector	References
WSB	Wilkes Basin	V-shaped	s, c, n	DX		54
ASB	Aurora Basin	V-shaped	s, c, n	SX		54
ST1			c	DX		
ST2			c	DX		
ST3		V-shaped	c, n	DX	yes	
ADV	Adventure Subglacial Trench	V-shaped	c	DX	yes	55
ST4		V-shaped	c, n	SX		
PEA	Peacock Subglacial Trench		c	SX		55
AUR	Aurora Subglacial Trench	V-shaped	c	SX		
VOS	Vostok Lake Subglacial Trench	V-shaped	c	SX	yes	
90E	90°E Lake Subglacial Trench		c	SX		56
sEEARS	Eastern East Antarctic Rift (southern segment)		s	SX		8
cEEARS	Eastern East Antarctic Rift (central segment)		c	SX	yes	8
nEEARS	Eastern East Antarctic Rift (northern sector)		n	SX		8
WEARS	Western East Antarctic Rift		s	SX		8
EAB	Eastern Basin		n	DX		16
CEB	Central Basin		n	DX		16
WEB	Western Basin - Webb Basin		n	DX		16
AST	Astrolabe Subglacial Basin		n	DX		56
FRO	Frost Subglacial Basin	V-shaped	n	DX	yes	57
ST5		V-shaped	n	DX	yes	
SAB	Sabrina Subglacial Basin	V-shaped	n	SX	yes	57
ST6			n	SX		
ST7			n	SX		
ST8			n	SX		
SHM	Shmidt Subglacial Basin		n	SX		58
KNO	Knox Subglacial Basin		n	SX		57
ST9			n	SX		
SB1		V-shaped	n	SX	yes	
LAM	Lambert Graben		n	SX		59

Extended Data Tab. 1

Shape: the term “V-shaped” is used to describe the pronounced convergence of the basin bounding faults toward a pivot point or pole. Annulus: southern sTAN (s), central cTAN (c) and northern nTAN (n) Transantarctic Annulus of the EAFBP in which the basin is located. Sector: dextral (DX) or sinistral (SX) EAFBP sector in which the basin is located. Bisector: for basins marked ‘yes’, the bisector of the triangular basin was used rather than the two longitudinal edges in the computation of the Euler Pole (see Methods). The acronyms SBn and STn (where n is an integer) are used for unnamed subglacial basins and trenches respectively.

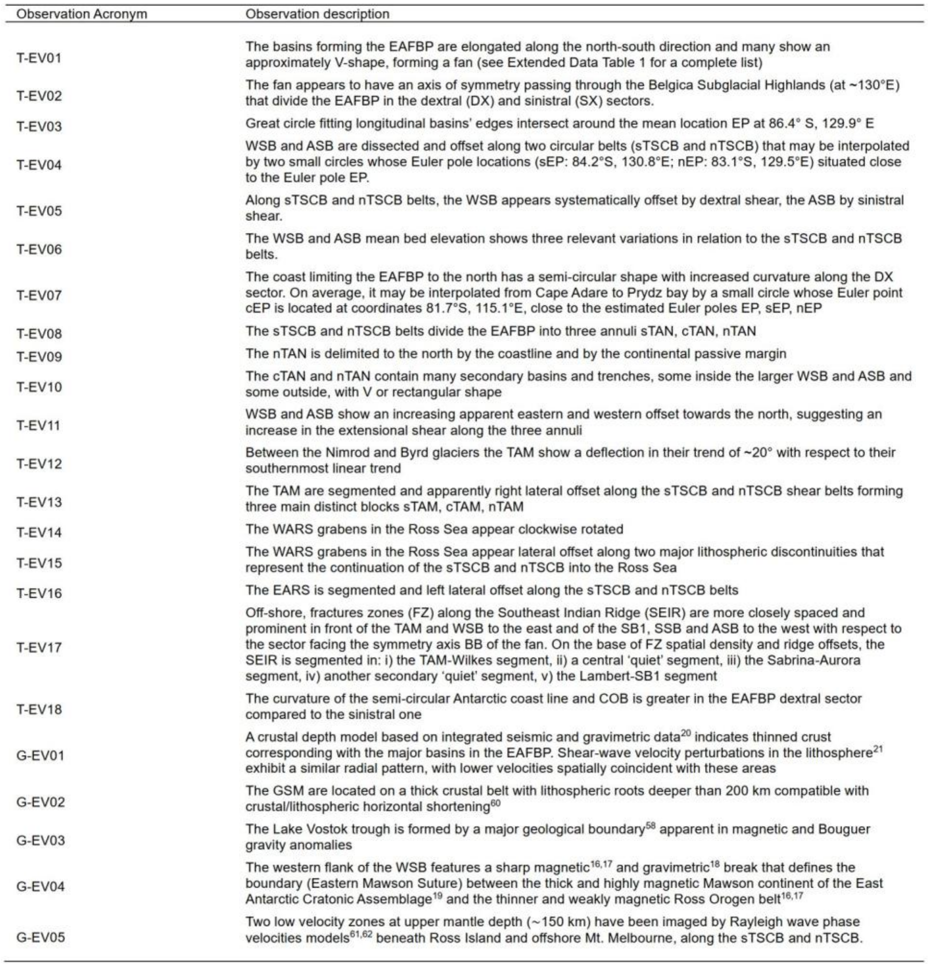

Observation Acronym	Observation description
T-EV01	The basins forming the EAFBP are elongated along the north-south direction and many show an approximately V-shape, forming a fan (see Extended Data Table 1 for a complete list)
T-EV02	The fan appears to have an axis of symmetry passing through the Belgica Subglacial Highlands (at ~130°E) that divide the EAFBP in the dextral (DX) and sinistral (SX) sectors.
T-EV03	Great circle fitting longitudinal basins' edges intersect around the mean location EP at 86.4° S, 129.9° E
T-EV04	WSB and ASB are dissected and offset along two circular belts (sTSCB and nTSCB) that may be interpolated by two small circles whose Euler pole locations (sEP: 84.2°S, 130.8°E; nEP: 83.1°S, 129.5°E) situated close to the Euler pole EP.
T-EV05	Along sTSCB and nTSCB belts, the WSB appears systematically offset by dextral shear, the ASB by sinistral shear.
T-EV06	The WSB and ASB mean bed elevation shows three relevant variations in relation to the sTSCB and nTSCB belts.
T-EV07	The coast limiting the EAFBP to the north has a semi-circular shape with increased curvature along the DX sector. On average, it may be interpolated from Cape Adare to Prydz bay by a small circle whose Euler point cEP is located at coordinates 81.7°S, 115.1°E, close to the estimated Euler poles EP, sEP, nEP
T-EV08	The sTSCB and nTSCB belts divide the EAFBP into three annuli sTAN, cTAN, nTAN
T-EV09	The nTAN is delimited to the north by the coastline and by the continental passive margin
T-EV10	The cTAN and nTAN contain many secondary basins and trenches, some inside the larger WSB and ASB and some outside, with V or rectangular shape
T-EV11	WSB and ASB show an increasing apparent eastern and western offset towards the north, suggesting an increase in the extensional shear along the three annuli
T-EV12	Between the Nimrod and Byrd glaciers the TAM show a deflection in their trend of ~20° with respect to their southernmost linear trend
T-EV13	The TAM are segmented and apparently right lateral offset along the sTSCB and nTSCB shear belts forming three main distinct blocks sTAM, cTAM, nTAM
T-EV14	The WARS grabens in the Ross Sea appear clockwise rotated
T-EV15	The WARS grabens in the Ross Sea appear lateral offset along two major lithospheric discontinuities that represent the continuation of the sTSCB and nTSCB into the Ross Sea
T-EV16	The EARS is segmented and left lateral offset along the sTSCB and nTSCB belts
T-EV17	Off-shore, fractures zones (FZ) along the Southeast Indian Ridge (SEIR) are more closely spaced and prominent in front of the TAM and WSB to the east and of the SB1, SSB and ASB to the west with respect to the sector facing the symmetry axis BB of the fan. On the base of FZ spatial density and ridge offsets, the SEIR is segmented in: i) the TAM-Wilkes segment, ii) a central 'quiet' segment, iii) the Sabrina-Aurora segment, iv) another secondary 'quiet' segment, v) the Lambert-SB1 segment
T-EV18	The curvature of the semi-circular Antarctic coast line and COB is greater in the EAFBP dextral sector compared to the sinistral one
G-EV01	A crustal depth model based on integrated seismic and gravimetric data[20] indicates thinned crust corresponding with the major basins in the EAFBP. Shear-wave velocity perturbations in the lithosphere[21] exhibit a similar radial pattern, with lower velocities spatially coincident with these areas
G-EV02	The GSM are located on a thick crustal belt with lithospheric roots deeper than 200 km compatible with crustal/lithospheric horizontal shortening[60]
G-EV03	The Lake Vostok trough is formed by a major geological boundary[58] apparent in magnetic and Bouguer gravity anomalies
G-EV04	The western flank of the WSB features a sharp magnetic[16,17] and gravimetric[18] break that defines the boundary (Eastern Mawson Suture) between the thick and highly magnetic Mawson continent of the East Antarctic Cratonic Assemblage[19] and the thinner and weakly magnetic Ross Orogen belt[16,17]
G-EV05	Two low velocity zones at upper mantle depth (~150 km) have been imaged by Rayleigh wave phase velocities models[61,62] beneath Ross Island and offshore Mt. Melbourne, along the sTSCB and nTSCB.

Extended Data Tab. 2

EAFBP: East Antarctic Fan-shaped Basin Province. GSM: Gamburtsev Subglacial Mts. TAM: Transantarctic Mts. sTSCB, nTSCB: southern and northern Transantarctic strike-slip Shear Circular Belts. WSB: Wilkes Subglacial Basin. ASB: Aurora Subglacial Basin.

References (main text)

1. Frémand, A.C. et al. Antarctic Bedmap data: FAIR sharing of 60 years of ice bed, surface and thickness data. *Earth System Science Data* **15**, 2695–2710 (2023), doi:10.5194/essd-15-2695-2023
2. Morlighem, M. et al. Deep glacial troughs and stabilizing ridges unveiled beneath the margins of the Antarctic ice sheet. *Nature Geoscience* **13**, 132-137 (2020), doi:10.1038/s41561-019-0510-8
3. Paxman, G.J.G., Austermann, J. & Hollyday, A. Total isostatic response to the complete unloading of the Greenland and Antarctic Ice Sheets. *Sci. Rep.* **12**, 11399 (2022), doi:10.1038/s41598-022-15440-y
4. Aitken, A.R.A. et al. Antarctic sedimentary basins and their influence on ice-sheet dynamics. *Reviews of Geophysics* **61**, e2021RG000767 (2023), doi:10.1029/2021RG000767
5. Paxman, G.J.G. et al. Bedrock erosion surfaces record former East Antarctic Ice Sheet extent. *Geophysical Research Letters* **45**, 4114–4123 (2018), doi:10.1029/2018GL077268
6. Storti, F., Holdsworth, R. E., Salvini, F. “Intraplate Strike-Slip Deformation Belts” in Intraplate Strike-Slip Deformation Belts, F. Storti, R. E. Holdsworth, F. Salvini, Eds., *Geological Society of London* (2003), pp. 1–14, doi:10.1144/gsl.sp.2003.210.01.01
7. Bo, S. et al. The Gamburtsev mountains and the origin and early evolution of the Antarctic Ice Sheet. *Nature* **459**, 690–693 (2009), doi:10.1038/nature08024
8. Ferraccioli F. et al. East Antarctic rifting triggers uplift of the Gamburtsev Mountains. *Nature* **479**, 388–392 (2011), doi:10.1038/nature10566.
9. Smith, A. & Drewry, D. Delayed phase change due to hot asthenosphere causes Transantarctic uplift? *Nature* **309**, 536–538 (1984), doi:10.1038/309536a0
10. Granot, R. & Dyment, J. Late Cenozoic unification of East and West Antarctica. *Nat. Commun.* **9**, 3189 (2018), doi:10.1038/s41467-018-05270-w
11. Paxman G.J.G. et al. The role of lithospheric flexure in the landscape evolution of the Wilkes Subglacial Basin and Transantarctic Mountains, East Antarctica. *Journal of Geophysical Research. Earth Surface* **124**, 812–829 (2019), doi:10.1029/2018JF004705
12. Siddoway, C. “Antarctica” in Encyclopedia of Geology, 2nd edition, S.A. Elias, D. Alderton, Eds., *Academic Press* (2021), pp. 642-658, doi:10.1016/B978-0-08-102908-4.00136-3
13. Goodge, J.W. Geological and tectonic evolution of the Transantarctic Mountains, from ancient craton to recent enigma. *Gondwana Research* **80**, 50-122 (2020), doi:/10.1016/j.gr.2019.11.001.
14. Cooper, A.K., Davey, F.J., Hinz, K. “Crustal extension and origin of sedimentary basin beneath the Ross Sea and Ross Ice Shelf, Antarctica” in Geological Evolution of Antarctica, M.R.A Thompson, J.A. Crame, J.W. Thompson, Eds., *Cambridge Univ. Press, New York* (1991), pp. 285-291
15. Boger, S.D. Antarctica - Before and after Gondwana. *Gondwana Research* **19**, 335-371 (2011), doi:10.1016/j.gr.2010.09.003.
16. Ferraccioli, F., Armadillo, E., Jordan, T., Bozzo, E., Corr, H. Aeromagnetic exploration over the East Antarctic Ice Sheet: a new view of the Wilkes Subglacial Basin. *Tectonophysics* **478**, 62-77 (2009), doi: 10.1016/j.tecto.2009.03.013
17. Golynsky, A.V. et al., New magnetic anomaly map of the Antarctic. *Geophysical Research Letters* **45**, 6437–6449 (2018), doi:10.1029/2018GL078153
18. Jordan, T.A., Ferraccioli, F., Armadillo, E., Bozzo, E. Crustal architecture of the Wilkes Subglacial Basin in East Antarctica, as revealed from airborne gravity data. *Tectonophysics* **585**, 196–206 (2013), doi:10.1016/j.tecto.2012.06.041.
19. Ruppel, A.S. et al., The Main Shear Zone in Sør Rondane, East Antarctica: Implications for the late-Pan-African tectonic evolution of Dronning Maud Land. *Tectonics* **34**, 1290–1305 (2015), doi:10.1002/2014TC003763.
20. Baranov, A., Tenzer, R. & Morelli, A. Updated Antarctic crustal model. *Gondwana Research* **89**, 1–18 (2021), doi:10.1016/j.gr.2020.08.010
21. Hansen, S.E. & Emry, E.L., East Antarctic tectonic basin structure and its implications for ice-sheet modeling and sea-level projections. *Commun Earth Environ,* **6**, 138 (2025). https://doi.org/10.1038/s43247-025-02140-4
22. Zwaan, F., Schreurs, G. & Rosenau, M. Rift propagation in rotational versus orthogonal extension: Insights from 4D analogue models. *Journal of Structural Geology* **135**, 103946 (2020), doi:10.1016/j.jsg.2019.103946

23. Zwaan, F. & Schreurs, G. Rift segment interaction in orthogonal and rotational extension experiments: Implications for the large-scale development of rift systems. *Journal of Structural Geology* **140**, 104119 (2020), doi:10.1016/j.jsg.2020.104119.
24. Schmid, T.S., Schreurs, G. & Adam, J. Characteristics of continental rifting in rotational systems: New findings from spatio temporal high resolution quantified crustal scale analogue models. *Tectonophysics* **822**, 229174 (2022), doi:10.1016/j.tecto.2021.229174
25. Parnell-Turner, R. & al. Causes and consequences of diachronous V-shaped ridges in the North Atlantic Ocean. Journal of Geophysical Research: Solid Earth **122**, 8675–8708 (2017). https://doi.org/10.1002/2017JB014225
26. Gibson, G. M., et al., Pre-existing basement structure and its influence on continental rifting and fracture zone development along Australia's southern rifted margin. *Journal of the Geological Society, London* **170**, 365–377 (2013). doi: 10.1144/jgs2012-040
27. Mouginot, J., Rignot, E. & Scheuchl, B. Continent-wide, interferometric SAR phase-mapping of Antarctic ice velocity. Geophysical Research Letters **46** (2019). DOI: 10.1029/2019GL083826.
28. Jamieson, S.S.R., Sugden, D.E. & Hulton, N.R.J. The evolution of the subglacial landscape of Antarctica. Earth and Planetary Science Letters **293**, 1–2, 1-27 (2010), https://doi.org/10.1016/j.epsl.2010.02.012.
29. Trench, D., Meigs, A. & Grunder, A. Termination of the northwestern Basin and Range province into a clockwise rotating region of transtension and volcanism, southeast Oregon. *Journal of Structural Geology* **39**, 52-65 (2012), https://doi.org/10.1016/j.jsg.2012.03.007.
30. Maritati, A., Danišík, M., Halpin, J. A., Whittaker, J. M., & Aitken, A. R. A. Pangea rifting shaped the East Antarctic landscape. Tectonics **39**, (2020), e2020TC006180. https://doi.org/10.1029/2020TC006180
31. Williams, S.E. et al. Australian-Antarctic breakup and seafloor spreading: Balancing geological and geophysical constraints. *Earth-Science Reviews* **188**, 41-58 (2019), doi:10.1016/j.earscirev.2018.10.011.
32. Eagles, G. A little spin in the Indian Ocean plate circuit. *Tectonophysics* **754**, 80-100 (2019), doi:10.1016/j.tecto.2019.01.015
33. Lisker, F. & Läufer, A.L. The Mesozoic Victoria Basin: Vanished link between Antarctica and Australia. *Geology* **41**, 1043–1046 (2013), doi:10.1130/G33409.1
34. Fitzgerald, P.G. & Goodge, J.W. Exhumation and tectonic history of inaccessible subglacial interior East Antarctica from thermochronology on glacial erratics. Nat Commun **13**, 6217 (2022). https://doi.org/10.1038/s41467-022-33791-y
35. Baranov A.A. & Lobkovsky L.I. Geodynamic processes, Cenozoic rifting and the mechanism of formation of the deepest depressions on land in Antarctica. Journal of Mining Institute **273**, 16614 (2025), 15-25. https://pmi.spmi.ru/pmi/article/view/16614
36. Granot, R., Cande, S. C., Stock, J. M. & Damaske, D. Revised Eocene-Oligocene kinematics for the West Antarctic rift system. *Geophys. Res. Lett.* **40**, 279–284 (2013). https://doi.org/10.1029/2012GL054181
37. Tikku, A.A. & Cande, S.C. The oldest magnetic anomalies in the Australian-Antarctic Basin: Are they isochrons? *J. Geophys. Res.* **104(B1)**, 661–677 (1999), doi:10.1029/1998JB900034.
38. Jacob, J. & Dyment, J. Early opening of Australia and Antarctica: New inferences and regional consequences. *Tectonophysics* **636**, 244-256 (2014), doi:10.1016/j.tecto.2014.08.020
39. White, L.T., Gibson, G.M. & Lister, G.S. A reassessment of paleogeographic reconstructions of eastern Gondwana: Bringing geology back into the equation. *Gondwana Research* **24**, 984-998 (2013), doi:10.1016/j.gr.2013.06.009.
40. Decesari, R.C., Wilson, D.S., Luyendyk, B.P., Faulkner, M. Cretaceous and Tertiary extension throughout the Ross Sea, Antarctica. *USGS Short Research Paper* **098**, USGS OF-2007-1047 (2007), doi:0.3 33/of2007-1047.srp098
41. Wilson, T.J. Cenozoic structural segmentation of the Transantarctic Mountains rift flank in southern Victoria Land. *Global and Planetary Change* **23**, 105-127 (1999), doi:10.1016/S0921-8181(99)00053-3.
42. Cox, S.C. et al. A continent-wide detailed geological map dataset of Antarctica. *Sci. Data* **10**, 250 (2023), doi:10.1038/s41597-023-02152-9.
43. Matthews, K.J., Müller, R.D., Wessel, P. & Whittaker, J.M. The tectonic fabric of the ocean basins. *J. Geophys. Res.* **116**, B12109 (2011), doi:10.1029/2011JB008413
44. Wolfson-Schwehr, M., Boettcher, M.S. "Global Characteristics of Oceanic Transform Fault Structure and Seismicity" in Transform Plate Boundaries and Fracture Zones, J.C. Duarte, Ed., *Elsevier* (2019), pp. 21-59, doi:10.1016/B978-0-12-812064-4.00002-5

45. NOAA National Centers for Environmental Information. ETOPO 2022 15 Arc-Second Global Relief Model. NOAA National Centers for Environmental Information. (2022), DOI: 10.25921/fd45-gt74. Accessed 12/03/2025
46. Gaina, C., Müller, R.D., Brown, B., Ishihara, T. & Ivanov, S. Breakup and early seafloor spreading between India and Antarctica. *Geophysical Journal International* **170**, 151–169 (2007), doi:10.1111/j.1365-246X.2007.03450.x
47. Müller, R.D. et al. A global plate model including lithospheric deformation along major rifts and orogens since the Triassic. *Tectonics* **38**, 1884–1907 (2019), doi:10.1029/2018TC005462
48. Seton, M. et al. A global data set of present-day oceanic crustal age and seafloor spreading parameters. *Geochemistry, Geophysics, Geosystems* **21**, e2020GC009214 (2020), doi:10.1029/2020GC009214
49. Müller, R.D. et al. Ocean basin evolution and global-scale plate reorganization events since Pangea breakup. *Annual Review of Earth and Planetary Sciences* **44**, 107-138 (2016), doi:10.1146/annurev-earth-060115-012211.

METHODS

Sub-ice topography isostatic adjustment

For the Antarctic bed topography, we used version 3 of the BedMachine compilation[2]. BedMachine derives bed elevation and ice thickness using a combination of mass conservation in regions of fast ice flow along the periphery of the ice sheet and streamline diffusion to interpolate between radio-echo sounding line data in the slow-moving interior. The nominal resolution of the BedMachine grid is 500 m, but we down-sampled this to 5000 m to facilitate faster computation. We then adjusted the topography for the isostatic effect of completely removing the modern ice sheet load (Extended Data Figure 1). For this, we used a pre-existing calculation[3], which computes the flexural response to the complete removal of the modern grounded ice load[2] using an elastic plate model with a laterally variability flexural rigidity, that also accounts for the disequilibrium associated with the ongoing response to ice mass changes since the Last Glacial Maximum. For simplicity, we referenced our rebounded topography to modern global mean sea level. We did not make any adjustments for post-34 Ma erosion, sedimentation, or associated isostatic adjustments, since correcting for these processes tends to smooth the topography, whereas the focus of this study is detecting changes in slope associated with tectonic structures.

Basin-edge detection

In order to trace the edges of the topographic subglacial basins within the EAFBP, we first applied a non-linear terracing filtering procedure to remove smooth, low-amplitude signals from the topography while preserving the sharper and higher-amplitude topographic variations. For an original topography, t0, and a filtered output topography, t, covering an area A, the procedure is based on an iterative algorithm that minimizes the Tikhonov parametric functional $T^{\alpha}(t)$, which is the weighted sum (by factor α) of two components:

$$T^{\alpha}(t) = \varphi(t) + \alpha \cdot S_{mgs}^{\beta}(t)$$

Where:

$\varphi(t)$ is a misfit functional determined as the norm of difference between true (t0) and output filtered (t) topography; it controls the closeness of the filtered output t to the original input topography t0:

$$\varphi(t) = \|t_0 - t\|$$

$S_{mgs}^{\beta}(t)$ is the minimum gradient support functional[51] defined as

$$S_{mgs}^{\beta}(t) = \int_A \frac{\nabla t \cdot \nabla t}{\nabla t \cdot \nabla t + \beta^2} dA$$

In this equation, the terms where the gradient ∇t is much less than β have zero contribution, while terms where any gradient much larger than β exists have contributions equal to one. Thus, sharp boundaries in topography are promoted and, consequently, enhancement of the edges of the basins, which are associated with steep topographic gradients, are obtained.

We then highlighted the strong variations in topography, that are expected to coincide with the flanks of the basins, by computing the magnitude of the horizontal gradient. The lineaments were then traced manually following the most prominent peaks. The process was assisted by automatic procedures such as the use of the phase congruency operator[52] to trace the local positive picks and the Hough transform to trace the correspondent lineaments[53]. The final set of basin edges (Fig. 1) is the result of this automatic procedure mixed with careful visual inspection and manual corrections. On the basis of the results, we identified 30 basins that are listed in Extended Data Table 1.

Estimation of the Euler poles

The Euler pole describing the rigid rotations that formed the EAFBP was estimated from the longitudinal edges of the basins that are expected to align along great circles that intersect at the Euler pole, which can also be visualized as the pivot point of the fan. First, we fitted the longitudinal edges of the basins to great circles in a least square sense and computed all the intersections between the extrapolations of these circles on a 3D Earth (Extended Data Figure 2). For some of the basins with triangular shape (see Extended Data Table 1), we interpolated a great circle along the bisector instead of the longitudinal edges. We considered 60 great circles and obtained 1103 intersections (Extended Data Figure 2), excluding those to the north of the EAFBP. Not all the intersections may be considered representative of the EAFBP Euler pole, since the direction of some of the basins' edges may have been strongly affected by inherited discontinuities or some of the basins may have not been formed in association with the EAFBP. Therefore, we applied an iterative scheme to remove outliers defined as the intersections that are more than three scaled median absolute deviations (MAD) far from the pole, obtaining the final 1025 intersections after 12 iterations. The Euler pole with coordinates 86.4°S, 129.9°E (WGS84) was estimated as the mean point of the final intersections. The ellipse error was computed as the area containing 68% of the intersections (resulting ellipse semiaxes: 750 and 330 km; azimuth of the major semiaxis at the EP: N8.9°W).

The two poles sEP (84.2°S, 130.8°E WGS84) and nEP (83.1°S, 129.5°E WGS84) for the southern and northern Transantarctic strike-slip Shear Circular Belts were estimated looking for the two small circles on the spherical Earth that are closer (in the least square sense) to the structural features defining the two belts shown in Extended Data Figure 2. The pole cEP (81.7°S, 115.1°E WGS84) for the coast was estimated looking for the small circle on the spherical Earth that is closer (in the least square sense) to the coastline between Cape Adare and Prydz Bay (Fig. S2).

Data availability

The filtered rebounded topography and detected lineaments that support the findings of this study are available in https://doi.org/10.6084/m9.figshare.25450219 (ref. 63).

The Antarctic bed topography is available in https://doi.org/10.5067/FPSU0V1MWUB6 (ref. 64).

The rebounded Antarctic bed topography is available in https://doi.org/10.18739/A2280509Z (ref. 65).

The ETOPO global relief model is available in https://doi.org/10.25921/fd45-gt74 (ref. 45).

The GEOMAP data set is available at https://doi.org/10.1594/PANGAEA.951482 (ref. 66).

The MEaSUREs Antarctic ice velocity data set is available in: https://doi.org/10.5067/PZ3NJ5RXRH10 (ref. 67).

The MEaSUREs Antarctic ice basin divides are available in: https://doi.org/10.5067/AXE4121732AD. (ref. 68).

The aeromagnetic ADMAP2 data set is available in: https://doi.org/10.1594/PANGAEA.892724 (ref. 69)

The updated CRUST 1.0 model with new data for Antarctica is available in https://data.mendeley.com/datasets/j58mf2wm9b/1 (ref. 70)

The 3-D shear-wave velocity model of Antarctica is available in: https://doi.org/10.17611/dp/emc.2025.anthansenemry2025.1 (ref. 71).

Code availability

Scripts used to support the analysis of topographic data are available in https://doi.org/10.6084/m9.figshare.25450219 (ref. 63).

References (Methods, Extended Data)

50. Morlighem, M. MEaSUREs BedMachine Antarctica. (NSIDC-0756, Version 3). Boulder, Colorado USA. NASA National Snow and Ice Data Center Distributed Active Archive Center. https://doi.org/10.5067/FPSU0V1MWUB6.
51. Portniaguine, O. & Zhdanov, M.S. Focusing geophysical inversion images. *Geophysics* **64**, 874-887 (1999), doi:10.1190/1.1444596
52. Kovesi, P., Image features from phase congruency. *Videre: A Journal of Computer Vision Research* **1(3)**, article 1 (1999).
53. Ghirotto, A. et al. The sub-ice structure of Mt. Melbourne Volcanic Field (Northern Victoria Land, Antarctica) uncovered by high-resolution aeromagnetic data. *Journal of Geophysical Research: Solid Earth* **128**, e2022JB025687 (2023), doi:10.1029/2022JB025687
54. Drewry, D.J. Sedimentary basins of the East Antarctic craton from geophysical evidence. Tectonophysics 36, 301-314 (1976), doi:10.1016/0040-1951(76)90023-8
55. Drewry, D.J. Antarctica: Glaciological and Geophysical Folio. Scott Polar Res. Inst., University of Cambridge (1983).
56. Siegert, M.J., Carter, S., Tabacco, I., Popov, S. & Blankenship, D. A revised inventory of Antarctic subglacial lakes. Antarct. Sci. 17, 453–460 (2005) doi:10.1017/S0954102005002889
57. Aitken, A.R.A. et al. The subglacial geology of Wilkes Land, East Antarctica. Geophys. Res. Lett. 41, 2390–2400 (2014), doi:10.1002/2014GL059405.
58. Leonov, V.O. & Popov, S.V. Geological Structure of Central East Antarctica from Geophysical Data. Geotectonics 43, 274–282 (2009).
59. Ravich, G.M., Soloviev, D.S. & Fodorov, L.V. Geologicheskoie Stroienie Zemli Mak-Robertsona (Vostochnaia Antarctida). Gidrometoizdat (1978)
60. An, M. et al. S-velocity model and inferred Moho topography beneath the Antarctic Plate from Rayleigh waves. J. Geophys. Res. Solid Earth 120, 359–383 (2015), doi:10.1002/2014JB011332
61. Graw, J.H. et al. Upper mantle shear wave velocity structure beneath northern Victoria Land, Antarctica: Volcanism and uplift in the northern Transantarctic Mountains. Earth and Planetary Science Letters 449, 48–60 (2016), doi:10.1016/j.epsl.2016.05.026
62. Hansen, S.E., Kenyon, L.M., Graw, J.H., Park, Y. & Nyblade, A.A. Crustal structure beneath the Northern Transantarctic Mountains and Wilkes Subglacial Basin: Implications for tectonic origins. Journal of Geophysical Research 121, 812–825 (2016), doi:10.1002/2015JB012325
63. Armadillo, E. Data files and matlab functions associated to the manuscript: Basin formation in interior East Antarctica triggered by large-scale rotational extension, submitted to Nature Geoscience. figshare. Dataset (2026). https://doi.org/10.6084/m9.figshare.25450219
64. Morlighem, M. MEaSUREs BedMachine Antarctica, Version 3. Boulder, Colorado USA. NASA National Snow and Ice Data Center Distributed Active Archive Center (2022). https://doi.org/10.5067/FPSU0V1MWUB6.
65. Paxman, G., Austermann, J., Hollyday, A. Grid files of the total isostatic response to the complete unloading of the Greenland and Antarctic Ice Sheets (version 1). Arctic Data Center (2022). https://doi.org/10.18739/A2280509Z
66. Cox, S. C. et al. The GeoMAP (v.2022-08) continent-wide detailed geological dataset of Antarctica. (2023) PANGAEA https://doi.org/10.1594/PANGAEA.951482.
67. Mouginot, J., E. Rignot, and B. Scheuchl. MEaSUREs Phase-Based Antarctica Ice Velocity Map, Version 1. Boulder, Colorado USA. NASA National Snow and Ice Data Center Distributed Active Archive Center. (2019). https://doi.org/10.5067/PZ3NJ5RXRH10.
68. Mouginot, J., B. Scheuchl, and E. Rignot. MEaSUREs Antarctic Boundaries for IPY 2007-2009 from Satellite Radar, Version 2. Boulder, Colorado USA. NASA National Snow and Ice Data Center Distributed Active Archive Center. (2017). https://doi.org/10.5067/AXE4121732AD.
69. Golynsky, A. V. et al. ADMAP2 Magnetic anomaly map of the Antarctic - links to files. PANGAEA (2018). https://doi.org/10.1594/PANGAEA.892724
70. Baranov, A. Data for: Updated CRUST 1.0 model with new data for Antarctica, Mendeley Data, V1, (2021), doi: 10.17632/j58mf2wm9b.1
71. Harris, S. & Emry, E. 3-D shear-wave velocity model of Antarctica from full-waveform ambient noise tomography (2025), https://doi.org/10.17611/dp/emc.2025.anthansenemry2025.1